11th International Symposium on Turbulence and Shear Flow Phenomena (TSFP11)
Southampton, UK, July 30 to August 2, 2019

ON THE RELATIONSHIP BETWEEN DRAG MODIFICATION AND VERTICAL VELOCITY FLUCTUATIONS IN FLOW OVER RIBLETS

Simone Di Giorgio
Dipartimento di Ingegneria Meccanica e Aerospaziale
Sapienza Università di Roma
Via Eudossiana 18, 00184, Roma
email simone.digiorgio@uniroma1.it

Sergio Pirozzoli
Dipartimento di Ingegneria Meccanica e Aerospaziale
Università La Sapienza
Via Eudossiana 16, I-00184, Roma
email sergio.pirozzoli@uniroma1.it

Stefano Leonardi
Department of Mechanical Engineering, University of Texas at Dallas
800 West Campbell Rd., Dallas, TX
email stefano.leonardi@utdallas.edu

Paolo Orlandi
Dipartimento di Ingegneria Meccanica e Aerospaziale
Università La Sapienza
Via Eudossiana 16, I-00184, Roma
email paolo.orlandi@uniroma1.it

ABSTRACT

We carry out DNS of flow over triangular and rectangular riblets in a wide range of size and Reynolds number, with the goal of establishing the mechanisms controlling drag reduction. It is found that drag reduction is primarily associated with the capability of inhibiting vertical velocity fluctuations at the plane of crests, as in SHS/LIS devices. This is efficiently achieved in DNS by artificial suppression of v, which yields large drag decrease, proportional to the riblets size. A parametrization of the drag reduction effect in terms of the vertical velocity variance is found to be quite successful to account for variation of the controlling parameters. A Moddy-like diagram is introduced which incorporates the effect of slip velocity and a single,geometry-dependent parameter. Lower drag-reduction efficiency of SHS/LIS-like riblets is found as compared to cases with artificially imposed slip velocity.

Introduction

Drag reduction is one of the primary goals in engineering fluid dynamic design, and for instance viscous drag due to turbulent boundary layers is a significant factor contributing to the aircraft fuel cost. Several studies have suggested that micro-surface wall geometry variations which change the near-wall structure of the flow are effective in reducing drag, as is the case of riblets (Walsh, 1986). Choi *et al.* (1993) carried out direct numerical simulation (DNS) of turbulent flows over riblet-mounted surfaces, achieving 6% drag reduction with triangular riblets with spanwise spacing in wall units $s^+ \approx 20$, and drag increase with $s^+ \approx 40$. García-Mayoral & Jiménez (2011) claimed that good characterization of the riblets performance breakdown may be obtained using the groove cross sectional area A_g^+, rather than the riblets spacing. In particular, they asserted that optimal performance of riblets is achieved for $\ell_g^+ = A_g^{+(1/2)} \approx 11$, regardless of the riblets shape. Many geometries and sizes of riblets have been studied numerically and experimentally, and maximum drag reduction is achieved of about 9%. The best results are typically obtained with sharp, blade-shaped riblets, which however are difficult to construct and maintain at the Reynolds numbers of engineering interest. A strategy has been pursued in recent years to overcome the performance limit of riblets, which involves the use of superhydrophobic surfaces (SHS, Min & Kim, 2004) and liquid-infused surfaces (LIS, Arenas *et al.*, 2019). The effects of hydrophobic surfaces on skin-friction drag have been investigated through direct numerical simulation of turbulent channel flow (Min & Kim, 2004), in which the actual surface texture is replaced with a slip-boundary condition at

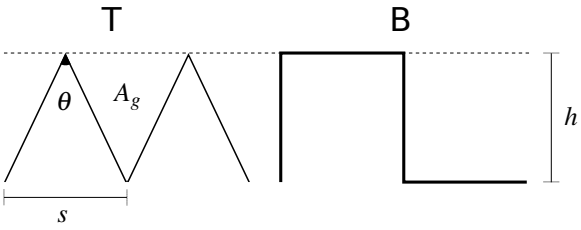

Figure 1. Sketch of the cross-stream profiles of triangular (T, left) and rectangular (R, right) riblets. The dashed lines marks the plane of crests.

the wall. Those authors showed that imparting a slip velocity in the streamwise and in the spanwise directions has quite a different effect on near-wall turbulence, resulting in large drag reduction in the former case, and large drag increase in the latter case. Arenas *et al.* (2019) carried out DNS of turbulent channel flow with two superposed fluids having different viscosity. Different textured surfaces were considered, with several values of the viscosity ratio. Large drag reduction was obtained with a staggered cubes pattern, which was connected with suppression of the wall-normal velocity fluctuations at the tip of the cubes. The importance of wall-normal velocity fluctuations in wall turbulence was previously emphasized by Orlandi & Leonardi (2008), who connected the drag increase effect in flow over rough walls with the r.m.s. of the vertical velocity at the plane of crests.

In this work we carry out DNS in a channel with triangular and rectangular riblets at the lower wall. Numerical simulations have been carried out by changing the riblets size and/or the bulk Reynolds number, also by suppressing the vertical velocity at the plane of crests, mimicking SHS and LIS. Besides a general study of the turbulence modification due to the presence of riblets, our goal is to establish whether a similar relationship between vertical velocity fluctuations and drag variation (with respect to the case of a smooth channel) as introduced by Orlandi & Leonardi (2008) for rough surfaces can also be traced in SHS and/or LIS.

Methodology

The numerical method relies on an incompressible second-order finite-difference solver with direct inversion of Poisson equation for the pseudo-pressure (Orlandi, 2012), which accounts for complex geometries through the immersed-boundary method. As proposed by Orlandi & Leonardi (2006), the no-slip condition at solid walls is satisfied by simply re-defining the metrics for derivative evaluation at the first layer of fluid points. DNS have been carried out in a channels with size $2\pi h \times 2h \times 1.25h$ in the streamwise, wall-normal and spanwise directions, by enforcing a constant mass flow rate, at bulk Reynolds number in the range $Re_b = 3,500 - 20,000$. A flat wall is assumed at the top boundary, whereas riblets are placed at the bottom wall. Triangular riblets with spanwise spacing $s = 0.125h$ and tip opening angle $\theta = 50.971\,[deg]$ have been considered as the baseline geometry (T1), for which a mesh with $256 \times 512 \times 512$ points has been used, yielding a resolution $\Delta x^+ \approx 6.9$, $\Delta z^+ \approx 1.4$ at $Re_b = 20,000$. Additional simulations, denoted as T2, have been carried out at fixed $Re_b = 5,600$ for geometrically similar triangular riblets with various spanwise spacing $s = 0.0415h, 0.083h, 0.166h$, (corresponding to $\ell_g = 0.03h, 0.06h, 0.12h$) on a $64 \times 384 \times 512$ mesh. Simulations of rectangular bars with the same spacing and height (hence the same gas fraction) as the T1 riblets have also been carried out using the same domain and grid, and referred to as B in the following (see Fig. 1). All DNS were repeated by forcing zero vertical velocity at the plane of crests, to mimic the conditions encountered in SHS or LIS with large surface tension, and referred to with the $V0$ suffix in the following. Finally, we have carried out for comparison a series of DNS of Couette-Poiseuille (CP) type flow by imparting a uniform slip velocity to the bottom wall (U_0) from $U_0 = 0.025U_b$ to $U_0 = 0.1U_b$, with Re_b from 4,000 to 15,000. These DNS have been performed on a $256 \times 384 \times 128$ mesh. The reference case of flow in a smooth channel is hereafter referred to as SM.

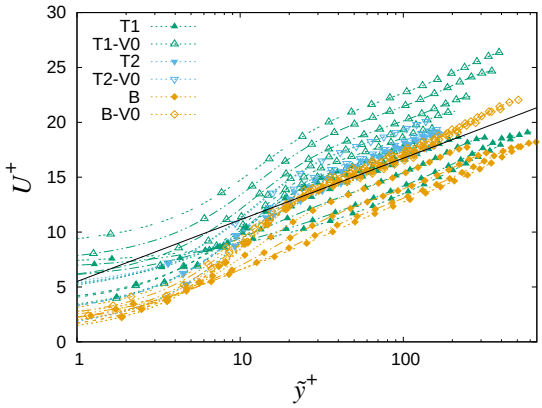

Figure 2. Inner-scaled velocity profiles near the rough wall (lines and symbols) as a function of distance from the plane of crests ($\tilde{y}$), for $T1$, $T2$, B, $T1-V0$, $T2-V0$, $B-V0$ simulations. Lines denote reference log law for low-Re flow, $U^+ = 1/k\log(y^+) + C$, $k = 0.41$, $C = 5.5$.

Results

Figure 2 shows the inner-scaled mean velocity profiles near the rough walls, where $\tilde{y}$ denotes the vertical distance from the plane of crests, and the bottom friction is estimated from mean momentum balance. Here U is the mean streamwise velocity, and the '+' superscript denotes normalization with either the friction velocity at the rough surface, or the associated viscous length scale. DNS data with standard no-slip boundary condition are shown in figure 2 with solid symbols, whereas cases with suppression of the vertical velocities at the riblets crest are shown with open symbols. Both cases with drag reduction (mean velocity above the reference log law at low Reynolds number, shown as a solid black line), and with drag increase (mean velocity below the log law) are present in figure 2. As pointed out by Rastegari & Akhavan (2015), the figure clearly brings out direct proportionality between mean velocity at the plane of the crests and the drag reduction effect. Standard riblets include four cases with drag reduction, specifically the $T1$ cases at $Re \le 5,000$, the $T2$ cases at $\ell_g \le 0.06$, whereas no drag reduction is found with the B geometry. It should be noted that drag reduction with longitudinal bars was previously reported by many authors (e.g. García-Mayoral & Jiménez, 2012), however with aspect ratio (thickness-to-spacing) $t/s = 0.25$, whereas we have $t/s = 1$. On the other hand, DNS with suppression of the vertical velocity yield an upward shift for all $T1-V0$ and $T2-V0$ cases, whereas it is only observed in the $B-V0$ cases at $Re \ge 10,000$. The

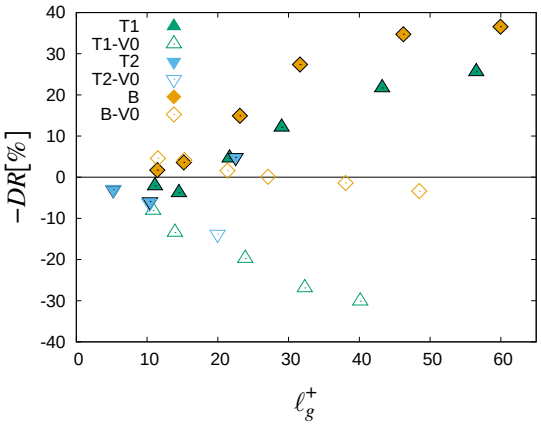

Figure 3. Percent drag reduction as a function of groove cross-sectional length scale in wall units.

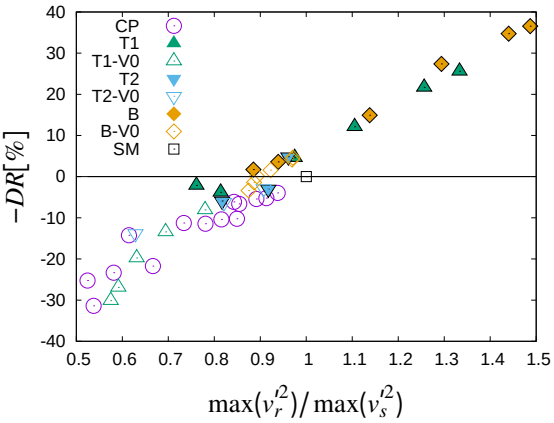

Figure 4. Percent drag reduction versus maximum vertical velocity variance, normalized with values at the smooth wall.

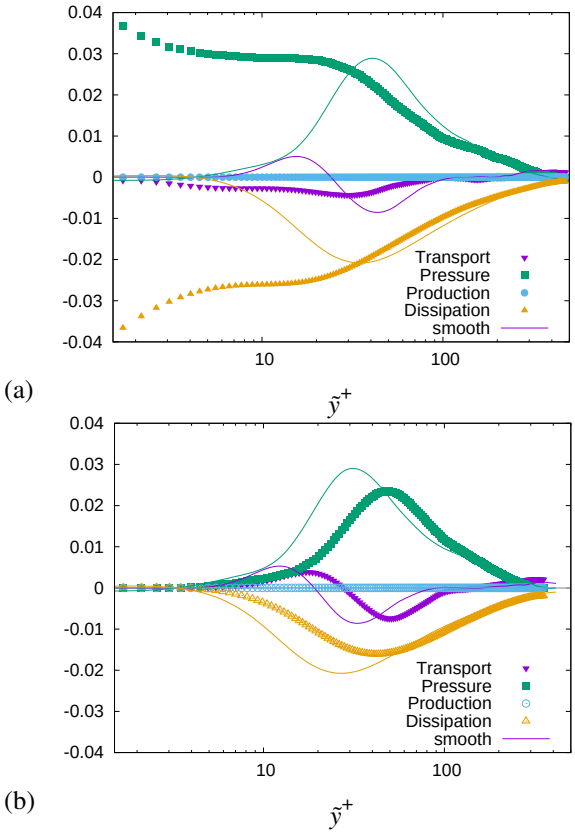

Figure 5. Budgets of vertical velocity variance for triangular riblets at $Re = 15{,}000$ (T1, panel (a)), and with suppression of vertical velocity at the plane of crests ($T1-V0$, panel (b)). Production, $-\langle u'v'\rangle \mathrm{d}U/\mathrm{d}y$; effective dissipation $\nu\langle u_i'\nabla^2 u_i'\rangle$; turbulent transport, $-\mathrm{d}\langle v'u_i'u_i'\rangle/\mathrm{d}y$; pressure tranfer, $-\mathrm{d}\langle p'v'\rangle/\mathrm{d}y$.

upward shift in these case is seen to steadily increase with the Reynolds number, consistent with observations made in previous work on SHS and LIS. On the other hand, when the vertical velocity at the plane of crests is not forced to be zero (cases T1, T2, B), the shift is generally downward, and it also increases with the Reynolds number, consistent with previous studies on rough walls (Perry *et al.*, 1969).

Figure 3 shows the relation between percent drag reduction, $DR = 1 - \tau_{wr}/\tau_{ws}$, and the typical groove length scale, ℓ_g^+. For the T1 and T2 test cases, our results are consistent with classical analysis (García-Mayoral & Jiménez, 2011), and maximum drag reduction is observed for T1 and T2 DNS at $\ell_g^+ \approx 11$, with subsequent saturation, and drag increase at large Reynolds number and/or riblets size. Since the B flow cases only yield drag increase, even for $\ell_g^+ \approx 11$, the bars geometry here considered may be regarded as belonging to the family of rough surfaces, rather than to riblets. Saturation of the drag reduction effect is prevented though enforcement of the zero vertical velocity condition in the $T1-V0$, $T2-V0$ and $B-V0$ simulations. In these cases the amount of drag reduction continues to be proportional to ℓ_g^+, thus supporting the effectiveness of technology capable of suppressing vertical velocities at the riblets crest, including SHS/LIS.

A parametrization for riblets and SHS/LIS devices has been recently proposed by Arenas *et al.* (2019), whereby the drag reduction effect is connected to the ratio of the maximum vertical velocity variance in the vertical direction at the 'rough' wall ($\max(v_r'^2)$) with respect to the smooth wall ($\max(v_s'^2)$). In figure 4 we report the percent drag reduction as a function of $\max(v_r'^2)/\max(v_s'^2)$, to show that variations in the roughness function also translate to drag reduction or increase, with a nearly linear, universal dependence. Figure 4 generally shows near proportionality between maximum vertical velocity fluctuations and drag reduction, supporting the statements of Arenas *et al.* (2019), and making it clear that drag reduction can only be achieved by reducing the intensity of the wall-normal velocity fluctuations. Here we further observe that the linear trend continues well into the rough wall regime, and that deviations from linearity arise for large drag reduction, with a possible lower limit for vertical velocity fluctuations. This is especially clear in the CP simulations, marked with open symbols.

In order to understand the effect of wall manipulation on the physics of the wall layer, in figure 5 we show the budgets of vertical velocity fluctuations for DNS of flow over T1 riblets at $Re = 15{,}000$ (panel (a)), which yields drag increase, and the corresponding DNS with suppression of v (panel (b)), which instead yields drag reduction. The figure well highlights that drag reduction through suppression of v does not cause substantial changes in the dynamics of the wall layer compared with the smooth wall case, however drag reduction is accompanied by reduction of all terms in the budget. On the other hand, drag increase is a associated with disruption of the wall layer organization. In particular, the pressure transfer term is maximum at the plane of crests,

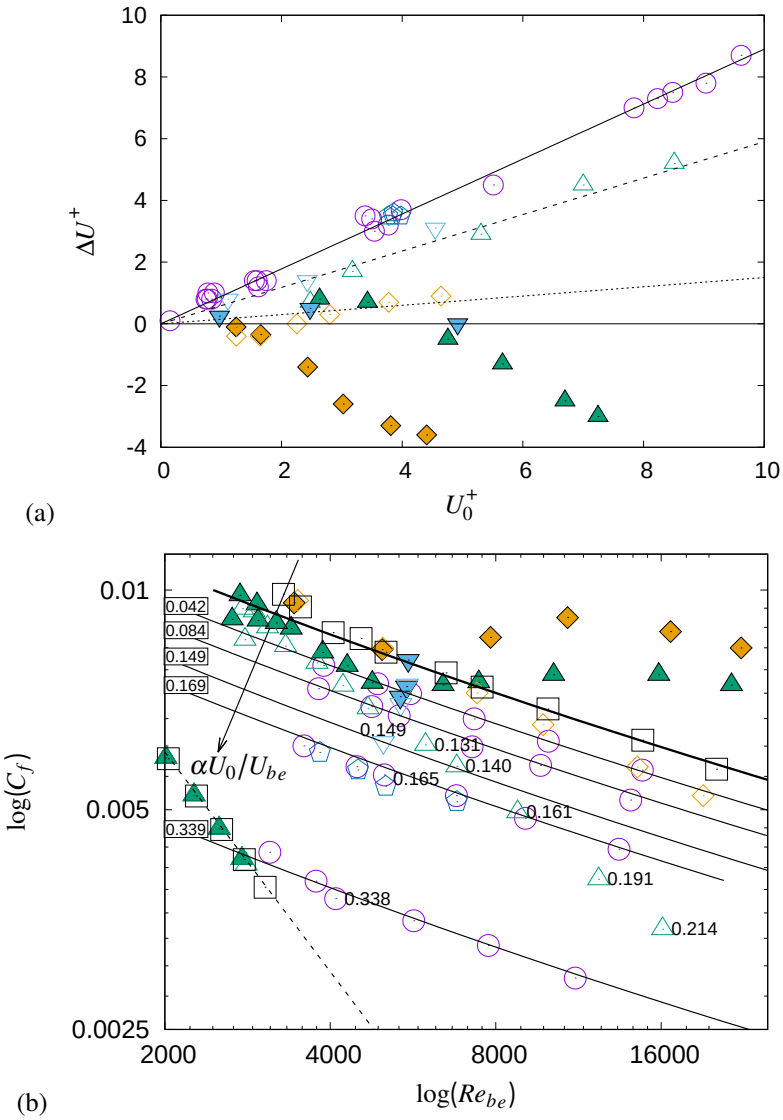

Figure 6. Relationship between roughness function and bottom wall slip velocity (a) and friction coefficient as a function of effective bulk Reynolds number (b) for flow cases SM (□), T1 (▲), T1-V0 (△), T2 (▼), T2-V0 (▽), B (◆), B-V0 (◇), CP (○), SIN (⬠). The solid black lines denote the analytical predictions of equation (3), for $\alpha U_0/U_{be} = 0, 0.042, 0.084, 0.149, 0.169, 0.339$ (from top to bottom). The dashed line denotes the friction law for laminar flow, $C_f = 12/Re_b$.

and it always acts to bring kinetic energy away from it.

We have previously shown (figure 3) that, by setting to zero the vertical velocity at the plane of crests, the riblets performance breakdown is prevented. In fact, suppression of the vertical velocities is equivalent to creating a slippery plane, thus replacing the no-slip boundary condition at the bottom wall with an axial velocity slip. However, the slip velocity is not uniform in the case of streamwise-aligned riblets, but rather varies along the spanwise direction, depending on the riblets shape and on the Reynolds number. Simulations with imparted sinusoidal spanwise variation of the slip velocity according to $U_0 \sin^2(\pi x)/2$, have thus been carried out to more closely replicate the mean velocity distribution observed in triangular riblets, which are referred to as SIN. In figure 6(a) we show a scatter plot of the roughness function ΔU^+ versus the mean slip velocity, U_0^+. Interestingly we find that, for a given riblet geometry, a linear relationship is present, namely $\Delta U^+ \approx \alpha U_0^+$, with geometry-dependent slope, which persists in all DNS with suppression of vertical velocity, whereas it is lost in the case of standard no-slip boundary condition, past the point of performance breakdown. The slope is seen to increase from $\alpha = 0.15$ for square bars, to about $\alpha = 0.59$ for triangular riblets, reaching the highest value $\alpha = 0.89$ for CP flow cases. Quite surprisingly, we find that the data for the SIN DNS have the same performance as the CP flow cases with uniform velocity, hence we find that spanwise modulation of the slip velocity has little effect on drag reduction. It should be pointed out that a universal linear relationship between drag reduction and slip velocity was observed by Rastegari & Akhavan (2015), based on the results of DNS with artificial slip/no-slip boundary conditions, assuming a flat wall. Very similar results are reported by those authors are here obtained in the CP DNS. We thus believe that the observed deviations from a universal law, with subsequent reduced drag-reduction efficiency are controlled by the actual wall geometry, although there is no mass communication between the bulk flow and the flow within the grooves. Equally important, the influence of the wall geometry geometry is distilled in the single parameter α, which may be

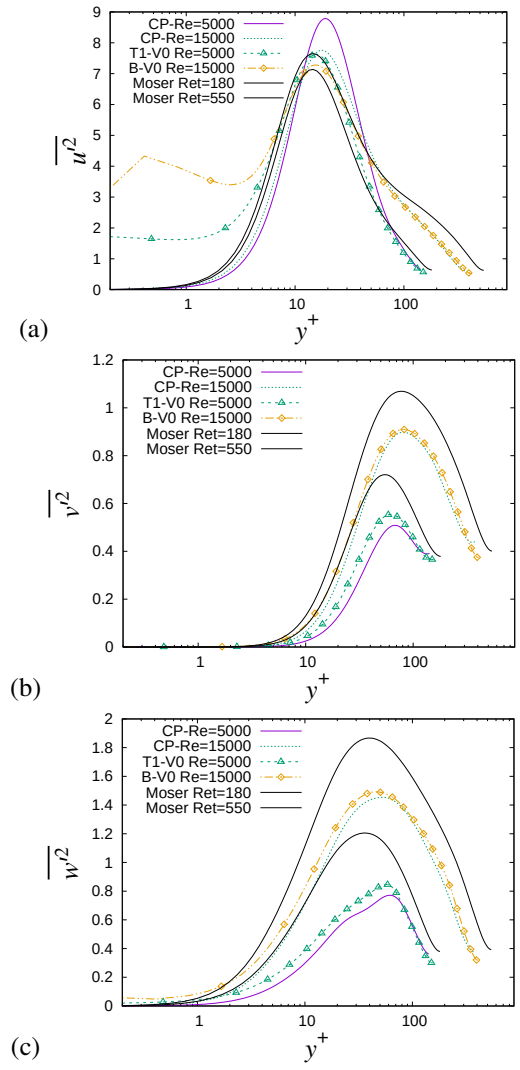

Figure 7. Wall-normal distributions of turbulence intensities.

determined once and for all.

The empirically determined relationship between ΔU^+ and U_0^+ can be profitably exploited to derive an analytical expression for the friction coefficient as a function of the bulk Reynolds number. For that purpose, we preliminarily introduce an effective height (h_e), as the difference between the point at which total stress is zero and the plane of crests ($y = y_0$), and an effective bulk velocity (U_{be}) in terms of the associated mass flow rate, namely

$$U_{be} = \frac{1}{h_e}\int_{y_0}^{h_e} U(y)\mathrm{d}y. \qquad (1)$$

As done for smooth channels, assuming that the mean velocity profile obeys a logarithmic law throughout,

$$U^+ = \frac{1}{k}\log y^+ + C + \Delta U^+ \approx \frac{1}{k}\log y^+ + C + \alpha U_0^+, \qquad (2)$$

and integrating in the vertical direction, one easily obtains

$$\sqrt{\frac{C_{fb}}{2}}\left(1-\alpha\frac{U_0}{U_{be}}\right)+\frac{1}{k}\log\left(2\sqrt{\frac{C_{fb}}{2}}\right)=\frac{1}{k}\left(\log(Re_{be}-1)\right)+C, \qquad (3)$$

whence the friction coefficient $C_f = 2/{U_{be}}^{+2}$ can be numerically obtained as a function of Re_{be} and U_0/U_{be}.

Figure 6(b) shows the friction coefficient versus the bulk Reynolds number as obtained from all DNS herein reported. The analytical trends predicted from equation (3) are also reported for increasing values of $\alpha U_0/U_b$ (solid lines), corresponding to drag reduction with respect to the smooth channel case, to obtain a Moody-like diagram. As expected, the behavior of friction in smooth channels (SM) is well reproduced from the laminar into the turbulent regime, with transition occurring between $Re = 3,000$ and $Re = 3,250$. As for the CP flow cases, they all show excellent agreement with the theoretical predictions, namely they all reside with minimal scatter, on the C_f curve corresponding to the respective $\alpha U_0/U_b$. Similar considerations can be made for the SIN cases, which are also found where predicted. Analyzing the behavior of riblets, some drag reduction is observed at transitional Reynolds numbers, with no substantial difference between non-slip and slip boundary conditions. Classical riblets are found to reach optimal performance for a specific number of Reynolds, past which they show increase and saturation of the friction coefficient in the fully rough regime. On the other hand the $V0$ simulations show a continuing trend for C_f to decrease with Re_b, at a rate which is well parametrized by equation (3). Once again, figure 6(b) confirms that wall movement in CP flow is the most efficient way to achieve drag reduction through wall slip. In order to understand the reduced efficient of V0 riblets with respect to CP flow, in figure 7 we compare distributions of the turbulence intensities along the coordinate directions, for flow cases yielding drag reduction. No substantial difference is in fact observed in the vertical and spanwise velocity fluctuations between CP flow and riblets. On the other hand, large differences are found toward the plane of crests in the streamwise velocity variance, which is quite large in riblets, and obviously zero in CP flow. Hence, we believe that poorer performance of riblets with impeded vertical velocity with respect to CP flows is the higher turbulent kinetic energy at the plane of crests, which must be sustained through additional power expenditure.

Conclusion

We have carried out a study of triangular and rectangular riblets in a wide range of riblet size and Reynolds number, also with suppression of the vertical velocity at the plane of crests. Consistent with previous studies, drag reduction of up to 9% is achieved with traditional riblets, making it difficult to construct and maintain them at Reynolds numbers of engineering interest. Drag reduction is found to be closely connected with suppression of turbulent stresses in the riblet grooves, which is effectively achieved by suppressing the vertical velocity, as is the case of super-hydrophobic or liquid-infused interfaces. Large drag reduction can then be achieved, which we find to be proportional to the change in the maximum vertical velocity variance, and associated with upward shift of the inner-scaled velocity profiles with respect to the case of smooth walls. Overall, we find that drag reduction can only be

achieved through control devices capable of suppressing v, in which case the near-wall layer dynamics is not modified. Consistent with previous work on SHS/LIS, we find clear association between the drag reduction effect and the presence of a slip velocity. In this respect, we have two interesting findings: i) in the case of a flat wall (CP flow), the actual spatial distribution of the slip velocity (U_0) is not important, but only its mean value; ii) in the presence of riblets with zero vertical velocity at the plane of crests, drag reduction is less than in the case of a flat wall, with direct effect of the wall geometry. The drag reduction effect due to wall slip is condensed in a single, geometry-dependent parameter (α) which we have used to obtain a Moody-like chart whereby the variation of the friction coefficient with the bulk Reynolds number is obtained, for assigned value of the parameter $\alpha U_0/U_b$.

REFERENCES

Arenas, I., Garcia, E., Orlandi, P., Fu, M., K., Hultmark, M. & Leonardi, S. 2019 Comparison between Super-Hydrophobic, Liquid Infused and rough surfaces: a DNS study. *J. Fluid Mech.* **869**, 500525.

Choi, H., Moin, P. & Kim, J. 1993 Direct numerical simulation of turbulent flow over riblets. *J. Fluid Mech.* **255**, 503539.

García-Mayoral, R. & Jiménez, J. 2011 Drag reduction by riblets. *Philos. T. Roy. Soc. A* **369** (1940), 1412–1427.

García-Mayoral, Ricardo & Jiménez, Javier 2012 Scaling of turbulent structures in riblet channels up to $\mathrm{re}_\tau \approx 550$. *Phys. Fluids* **24**, 105101.

Min, T. & Kim, J. 2004 Effects of hydrophobic surface on skin-friction drag. *Phys. Fluids* **16** (7), L55–L58.

Orlandi, Paolo 2012 *Fluid flow phenomena: a numerical toolkit*, , vol. 55. Springer Science & Business Media.

Orlandi, P. & Leonardi, S. 2006 DNS of turbulent channel flows with two-and three-dimensional roughness. *J. Turbul.* **7**, N73.

Orlandi, P. & Leonardi, S. 2008 Direct numerical simulation of three-dimensional turbulent rough channels: parameterization and flow physics. *J. Fluid Mech.* **606**, 399415.

Perry, A.E., Schofield, W.H. & Joubert, P.N. 1969 Rough wall turbulent boundary layers. *J. Fluid Mech.* **37**, 383–413.

Rastegari, A. & Akhavan, R. 2015 On the mechanism of turbulent drag reduction with super-hydrophobic surfaces. *J. Fluid Mech.* **773**, R4.

Walsh, M. J. 1986 Riblets for aircraft skin-friction reduction. *Tech. Rep.*. NASA Langley Research Center, Hampton, VA, United States).